Broadband NDSHA computations and earthquake ground motion observations for the Italian territory

Andrea Magrin*

Department of Mathematics and Geosciences,
University of Trieste,
Via E. Weiss, 4 Pal. P, Trieste I-34127, Italy
Email: andreamagrin@yahoo.it
*Corresponding author

Alexander A. Gusev

Institute of Seismology and Volcanology,
Far East Division, Russian Ac. Sci., Piip Blvd. 9,
Petropavlovsk-Kamchatsky 683006, Russia
and
Kamchatka Branch, Geophysical Survey,
Russian Ac. Sci., Piip Blvd. 9,
Petropavlovsk-Kamchatsky 683006, Russia
Email: gusev@emsd.ru

Fabio Romanelli and Franco Vaccari

Department of Mathematics and Geosciences,
University of Trieste,
Via E. Weiss, 4 Pal. P, Trieste I-34127, Italy
Email: romanel@units.it
Email: vaccari@units.it

Giuliano F. Panza

Department of Mathematics and Geosciences,
University of Trieste,
Via E. Weiss, 4 Pal. P, Trieste I-34127, Italy
and
China Earthquake Administration,
Institute of Geophysics,
Beijing, China
and
International Seismic Safety Organization (ISSO),
Viale San Francesco, 12, I-64031 Arsita (TE), Italy
and
Accademia Nazionale dei Lincei,
Palazzo Corsini – Via della Lungara, 10 – 00165, Rome, Italy
Email: giulianofpanza@fastwebnet.it

Abstract: The aim of this work is two-fold: 1) to compare the results of national scale NDSHA modelling for the Italian region at 10 Hz cut-off, based on the relevant available knowledge, with observations (e.g., peak ground motion values) and existing empirical attenuation relations; 2) to update the scaling law for source spectra (SLSS) to be used for the selected area. The new set of source spectra, defined along the lines suggested by the comparison with empirical attenuation relations, produces acceptable results in terms of PGV and spectral acceleration at long periods. Synthetic PGA and SA at short periods show a faster attenuation with respect to the observed ones and, therefore, the effect of complex attenuation factors should be explored in future ad hoc studies.

Keywords: synthetic seismograms; scaling law for source spectra; SLSS; modal summation; strong motion estimation; ground motion prediction equation; GMPE; NDSHA; earthquake scenarios; modelling; seismic hazard; ground motion observations; Italy.

Reference to this paper should be made as follows: Magrin, A., Gusev, A.A., Romanelli, F., Vaccari, F. and Panza, G.F. (2016) 'Broadband NDSHA computations and earthquake ground motion observations for the Italian territory', *Int. J. Earthquake and Impact Engineering*, Vol. 1, Nos. 1/2, pp.131–158.

Biographical notes: Andrea Magrin graduated in Physics at the University of Trieste, where he received his PhD in Geophysics of the Lithosphere and Geodynamics. He was a Post-doc Researcher at the Department of Mathematics and Geosciences (2013 to 2014) and Visiting Scientist at the ICTP ESP-SAND Group (2015). His main research topics are ground motion scenarios and seismic hazard estimation.

Alexander A. Gusev is the Group Head at the Institute of Volcanology and Seismology, Petropavlovsk-Kamchatsky in 1978 to 2016. He works in seismology and data analysis. His main results in earthquake source physics and source simulation, fractal properties of earthquake and eruption catalogues, scaling and fractal features of earthquakes and seismic wave field, modelling of random seismic wave generation and propagation and recovery of scattering properties of the Earth from high-frequency waves. He applied results in earthquake hazard analysis, strong motion data processing, real-time tsunami warning. He received a State Award of Russia (2002) for participation in the development of the official seismic zoning map of Russia of 1997.

Fabio Romanelli graduated in Physics at the University of Trieste, where he received his PhD in Geophysics. He is currently a Researcher in Seismology at the Department of Mathematics and Geosciences, and Professor of Seismology, Seismic Risk and Institutions of Physics of the Earth. His main research topics are: seismic and tsunami wave generation and propagation; ground shaking scenarios and seismic hazard estimation, definition of seismic input and estimation of parameters of seismic engineering importance; study of the lithosphere-asthenosphere system.

Franco Vaccari graduated in Geology at the University of Trieste in 1986, where he received his PhD in Geophysics of the Lithosphere and Geodynamics. He was a Research Fellow at the Gruppo Nazionale per la Difesa dai Terremoti (GNDT) under CNR (1990 to 1999) and at the Istituto Nazionale di Geofisica e Vulcanologia (INGV) (2000 to 2002), collaborator at the University of Trieste, Department of Earth Sciences (2003 to 2006), Contract Researcher at the

University of Trieste, Department of Mathematics and Geosciences (2007 to 2010) and Visiting Scientist at the ICTP ESP-SAND Group (1990 to 2015). His main research interests are: synthetic seismograms; seismic hazard assessment and seismic zoning; development of seismological software. He is the author of 120 publications, mostly on international, and peer-reviewed journals.

Giuliano F. Panza is a retired Professor of Trieste University. His research topics covered broad multidisciplinary nature of problems as simultaneous use of neo-deterministic seismic hazard assessment (NDSHA) and monitoring of space/time variation of hazard lead to the construction of time/dependent models of particular interest for civil defence. He received his EGU Beno Gutenberg Medal, Bucharest University Laurea H.C., Medals of Honour Central European Initiative and NRIAG Egypt, Commemorative Medal VAST Vietnam, H.Prof. IG/CEA Beijing, Accademia Nazionale dei Lincei, AE, TWAS, RAS and Accademia Nazionale delle Scienze, Knigth OMRI. He is an ESR Editor-in-Chief and JSEE Co-Editor. He ranks at #4 by papers (June 2010 SCIENCEWATCH.COM). In the Web of Science®, his record includes 109 original articles cited 715 times between January 2000 and May 2010.

1 Introduction

The procedure for the neo-deterministic seismic hazard assessment (henceforth named NDSHA) (Panza et al., 2001, 2012) is based on the definition of earthquake ground motion by means of the computation of synthetic seismograms, for a set of earthquake scenarios. NDSHA allows us to obtain a realistic estimate of the seismic hazard where scarce (or no) historical or instrumental information is available. Synthetic seismograms can be constructed to model ground motion at sites of interest, using knowledge of the physical process of earthquake generation and wave propagation in realistic media. The signals are efficiently generated by the modal summation technique (e.g., Panza et al., 2001), making it possible to perform detailed parametric analyses that permit to account for the uncertainty in input information. The method defines the hazard from the envelope of the values of ground motion parameters determined considering a wide set of scenario earthquakes; accordingly, the simplest outcome of this method is a map where the maximum of a given seismic parameter is associated to each site. The NDSHA procedure provides strong ground motion parameters based on the seismic wave propagation modelling at different scales – regional, national, and metropolitan – accounting for a wide set of possible seismic sources and for the available information about structural models. As described by Vaccari (2016), some packages devoted to NDSHA have been implemented as a web application (http://www.xeris.it/index.html).

NDSHA differs from the classical deterministic seismic hazard assessment (DSHA), since it computes earthquake ground motions as tensor product of the earthquake source tensor with the Green's function for the medium. Hence, NDSHA does not make use of ground motion prediction equations (GMPEs), which do not preserve the tensor nature of earthquake ground motion (as shown by Paskaleva et al., 2007). Contrary to probabilistic seismic hazard assessment (PSHA), this approach does not rely on the statistical characterisation of earthquake recurrence, which is severely restricted by the available observations. Rather, it makes use of information about the space distribution of large

magnitude earthquakes, which can be defined based on seismic history and seismotectonics, as well as incorporating information from a wide set of geological and geophysical data.

At a regional scale, synthetic seismograms are computed at sites placed at the nodes of a 0.2° × 0.2° grid that covers the national territory, considering the average structural model associated to the regional polygon that includes the site [e.g., the set of structural models from Brandmayr et al. (2010)]. When seismograms are computed for a cut-off frequency of 1 Hz, the earthquake can be adequately represented by a point source (approximation valid when the source-receiver distance is much greater than the source dimensions) scaled for its size using the relatively simple source spectra scaling laws (in the following size scaled point source, SSPS) of Gusev (1983), as reported in Aki (1987). The scaling law for source spectra (SLSS) proposed by Gusev (1983) (henceforth named G83), reasonably represents, from a qualitative and, to a certain degree, a quantitative point of view, seismic source data at a global scale, as successfully tested in particular by Boore (1986). However, it can be naturally updated, assimilating the new data recorded in the last decades, and, often, better tuned, when focusing to a specific area, where data of suitable quality are available.

As reported in Panza et al. (2012), where examples of computation with a cut-off frequency of 10 Hz are shown, the cut-off frequency of 1 Hz used in the generation of the synthetic seismograms is not a technical limitation of the computational algorithm, but a deliberate choice fully consistent with the SSPS approximation originally adopted in Panza et al. (2012). With the latest package of NDSHA programs (Panza et al., 2012), where the fault finiteness is duly taken into account, the cut-off frequency is readily increased to 10 Hz. A more realistic source model than SSPS can thus be naturally used to increase the cut-off frequency of computation of seismograms for the national scale maps. This allows us to exploit detailed structural information, wherever available, and to estimate the maximum acceleration (peak ground acceleration – PGA) directly from the time series.

The aim of this work is two-fold:

a to compare the results of national scale NDSHA modelling for the Italian region at 10 Hz cut-off, based on the relevant available knowledge, with observations (e.g., peak ground motion values) and existing empirical attenuation relations

b to update the SLSS to be used for the selected area.

Specifically, we consider the parameters determined using GMPEs derived from the Italian strong motion database, called in the following ITA08 (Bindi et al., 2010). Then, a new reference SLSS is defined along the lines suggested by this comparison. Even if NDSHA does not use attenuation relations, GMPE supply a simplified information (a sort of proxy datum) useful to test the NDSHA modelling procedure. The NDSHA-computed ground motion parameters are directly compared with a set of observed values, partially independent on the dataset used to derive ITA08. In this way, we can show that the definition of SLSS tuned during the first step does not need further adjustments when different datasets are considered.

Among the parameters representative of earthquake strong ground motion, we focus on the widely used PGA and spectral acceleration (SA) at different periods, and peak ground velocity (PGV), that is directly connected with energy demand and seems to be a more representative measure of earthquake intensity (e.g., Uang and Bertero, 1990;

Decanini and Mollaioli, 1998; Cosenza and Manfredi, 2000). The results acquired from the comparison between empirical and modelled PGA and PGV can be readily used to derive, by analytical integration, reliable predictions for peak ground displacement (PGD).

2 Computation of synthetic seismograms

In the NDSHA approach, the definition of the space distribution of seismicity accounts only for the largest events reported in the earthquake catalogue at different sites, as follows. As described more in details in Panza et al. (2001), earthquake epicentres reported in the catalogue are grouped into 0.2° × 0.2° cells, assigning to each cell the maximum magnitude recorded within it. A smoothing procedure is then applied to account for spatial uncertainty and for source dimensions. Only cells located within the seismogenic zones are retained. This procedure for the definition of earthquake locations and magnitudes for NDSHA makes the method pretty robust against uncertainties in the earthquake catalogue, which is not required to be complete for magnitudes lower than 5. A double-couple point source is placed at the centre of each cell, with a focal mechanism consistent with the properties of the corresponding seismogenic zone. Source depth is taken as a function of magnitude. Even if NDSHA can use information about the possible location of strong earthquakes provided by morphostructural analysis (Zuccolo et al., 2011), for the comparison between the NDSHA computed ground motion and GMPE related values, we consider only the sources falling into the seismogenic zones defined by Meletti et al. (2008) (see Figure 1), whose magnitudes are defined from the CPTI04 catalogue (CPTI Working Group, 2004).

To define the physical properties of the source-site paths, the territory is divided into 1.0° × 1.0° cells, each characterised by a 'cellular' structural model composed of flat, parallel anelastic layers that represent the average lithosphere properties at regional scale (Brandmayr et al., 2010), already used in Panza et al. (2012). Synthetic seismograms are then computed by the modal summation technique (MS henceforth) for sites placed at the nodes of a grid with step 0.2° × 0.2° that covers the national territory, considering the average structural model associated to the regional polygon that includes the site. The maximum source-site distance adopted in the calculations is 150 km for all the events.

A more realistic source model than the SSPS is necessary to raise the maximum frequency of computation of seismograms for national scale maps to 10 Hz. The use of extended source models, which take into account near source effects, can be considered too expensive in terms of computational time, when applied for seismic hazard assessment at a national scale, given the large number of seismograms to be computed for each source. Therefore, we have considered the size and time scaled point source (STSPS) model (Parvez et al., 2011), computed with PULSYN06 algorithm (Gusev, 2011) that provides a broadband kinematic source model. The extended source model is described in terms of a grid of sub point-sources (shortly subsources). The spectra of the subsources moment rate functions satisfy the condition to fit the reference SLSS and provide the basic elements necessary to describe realistically an extended source. They are summed in order to obtain a single source spectrum, representative of the entire space and time structure of the extended source in far source condition (STSPS), taking into account directivity effects. The starting reference SLSS used to compute seismograms is

G83 and the considered earthquake source model has unilateral rupture, with ratio between rupture velocity and velocity of S-wave equal to 0.8, at neutral directivity direction (90°) in a medium with S-wave velocity equal to 3.5 km/s.

Figure 1 (a) Focal mechanisms associated with the seismogenic zones ZS9 (Meletti et al., 2008) and (b) maximum magnitude (after smoothing, see Panza et al., 2001) of sources inside the seismogenic zones adopted for national scale computations

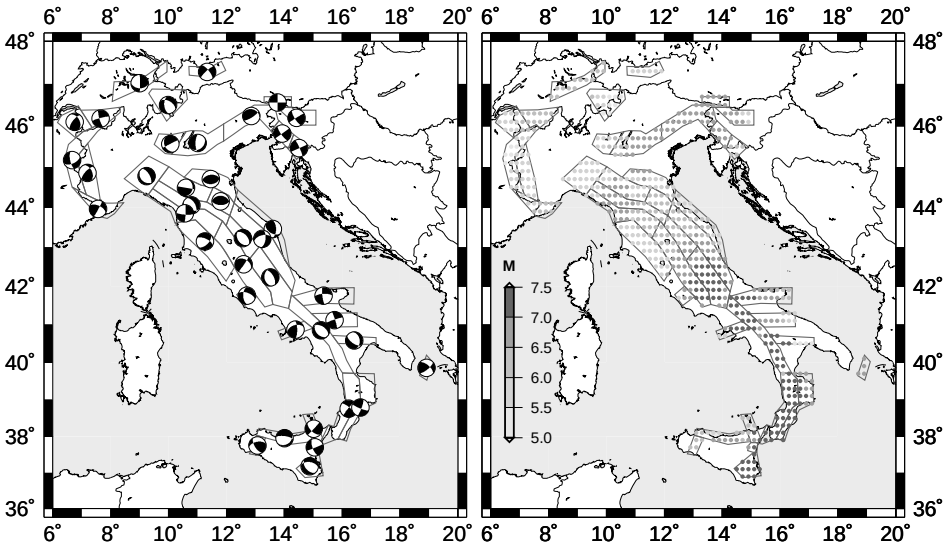

(a) (b)

The computation of realistic synthetic time-histories requires crustal models for P- and S-wave velocities, density and quality factor (Q), detailed as much as possible. On account of the existing information, the set of cellular structures (1.0° × 1.0°) of Brandmayr et al. (2010) is used: S-wave distribution with depth was obtained through an optimised nonlinear inversion of surface wave dispersion curves, (see Figure 2) and completed by independent information. Specifically, S-wave attenuation data come from studies of Martínez et al. (2009, 2010) for latitude lower than 45° and from Craglietto et al. (1989) from the rest of the cells. The values of P-wave attenuation (Q_P) has been derived using the popular relation $Q_P = 2.2 \cdot Q_S$ (Anderson, 2007). The MS technique is very fast and provides an accurate simulation of ground motion in the far field. The seismograms computed by MS contain all the body waves whose horizontal phase velocities are smaller than the S-wave velocity of the half-space that terminates the structural model used as input, and it should be used only to compute signals at epicentral distances greater than the focal depth. Therefore, MS is not appropriate for hazard scenarios in near source and near field condition. This limit of MS is easily bypassed using the discrete wave number technique (henceforth named DWN) (Pavlov, 2009), that gives the full wave field, including all body waves and near field, for computations at epicentral distances less than, or comparable with, the source depth.

Figure 2 Cellular structural models (Brandmayr et al., 2010) used for computation of synthetic seismograms

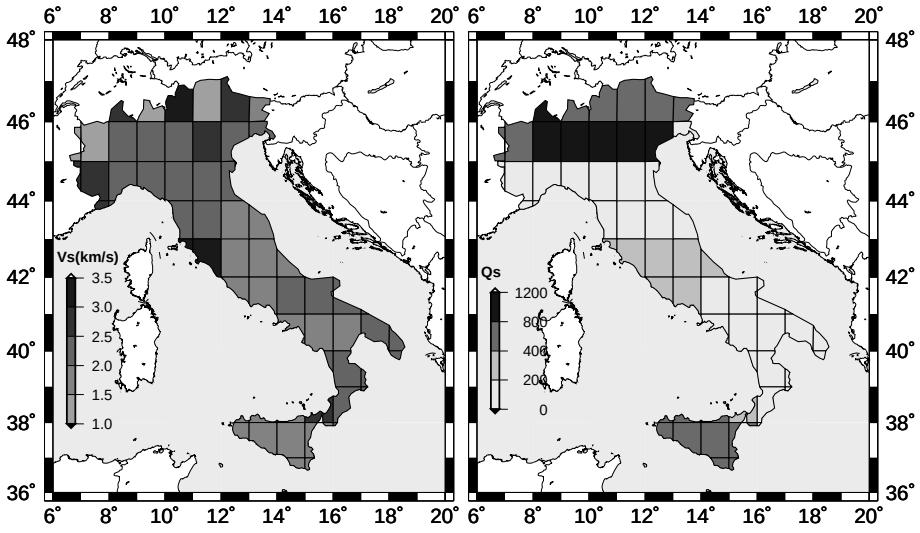

(a) (b)

Notes: The territory is divided into 1.0° × 1.0° cells, each characterised by a structural model composed of flat, parallel an elastic layers that represent the average lithosphere properties at regional scale. Properties of the uppermost layer of each cellular model are shown: (a) V_S and (b) Q_S.

3 Comparison of synthetic signals with GMPE 'ITA08'

The test is made against ITA08, GMPE determined by Bindi et al. (2010) who considered the strong motion records processed in ITACA (Luzi et al., 2008). Earthquakes with moment magnitude $M_W \geq 4$, and, recorded at least by two stations, at distances from the fault smaller than 100 km, are used. Bindi et al. (2010) adopt the same site classifications as Sabetta and Pugliese (1987), that consist of three classes: the first (C_0) includes the stations installed on rock, the second (C_1) includes the stations installed on shallow sediments (thinner than 20 m), the third (C_2) is representative of the stations installed on sediments thicker than 20 m, where with the term sediment are denoted soils with S-wave velocity lower than 0.8 km/s. The equations for the median have the following functional form:

$$\begin{aligned}\log_{10} Y = a + b_1 \left(M_W - M_{ref}\right) + b_1 \left(M_W - M_{ref}\right)^2 \\ + \left(c_1 + c_2 \left(M_W - M_{ref}\right)\right) \log_{10} \sqrt{\left(R^2 + h^2\right)} + e_i S_i + f_j F_j\end{aligned} \quad (1)$$

where Y is the ground motion parameter; M_{ref} is a reference magnitude; R is the distance; h is the pseudo-depth (km); S_i with i = 1, 2, 3 are dummy variables that assume either the value 0 or 1 depending on soil type; F_j are dummy variables that take either the value 0 or 1 depending on the style of faulting; e_i and f_j are the site and the style-of-faulting coefficients, respectively.

Figure 3 Comparison between synthetic PGA (computed with G83) (black) and PGA from ITA08 (grey) versus distance (km) for the magnitude classes 5.5, 6.0 and 6.5

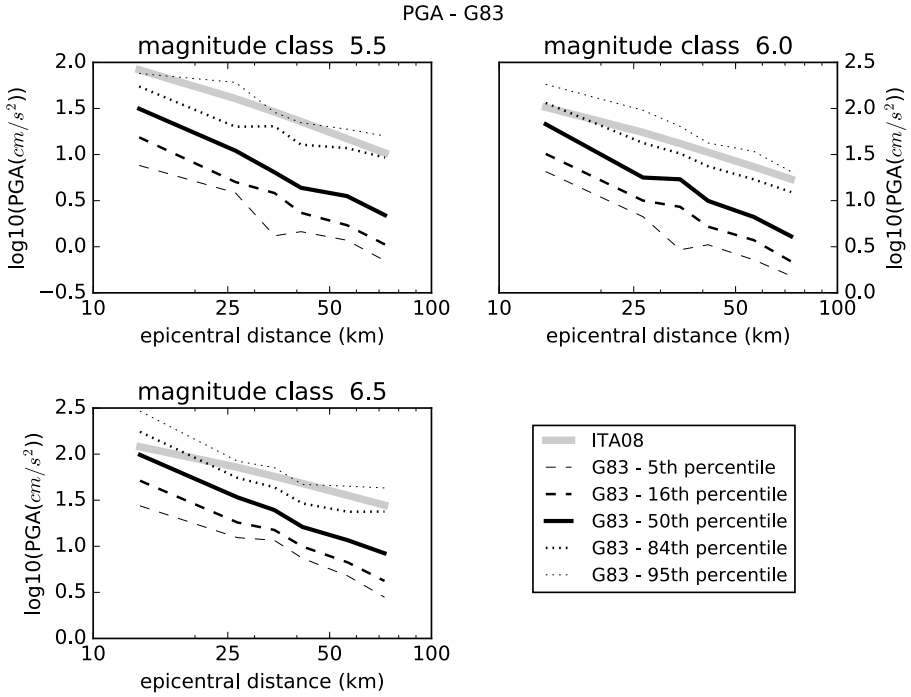

Note: The scatter of simulated PGA, reflected in the plot through quantile curves, results from the use of different focal mechanisms and different sites configurations.

We consider PGV and PGA of each seismogram computed to construct the NDSHA map. To take into account the uncertainties in magnitude determination, the (synthetic) peak values are grouped into six magnitude classes of the causative earthquakes with a step ΔM = 0.5, in the range 4.75–7.75. The dataset used for the determination of ITA08 includes events up to magnitude 6.9: thus, the comparison for magnitude classes 7.0 and 7.5 is not binding. Magnitude class 5.0 (4.75–5.25) contains only 136 synthetic seismograms (while in the others classes the population of signals exceeds 10,000). The peaks are also grouped into distance classes from the causative earthquakes that are controlled by the size of the grid where signals are computed in NDSHA. All the structural models used belong to C_0 class [see Figure 2(a)]; therefore, the synthetic peaks are compared with the GMPE determined for the (same) station class C_0 (rock). The scatter of simulated strong motion parameters, reflected in Figures 3 and 4 through quantile curves, results from the use of different focal mechanisms (Figure 1) and different sites configurations. Namely, each site lies in the pertinent structural model (Figure 2) and at a specific position with respect to the radiation pattern of the affecting focal mechanisms. The difference between the logarithms of the median of synthetic peaks and the corresponding values given by ITA08 equation will be called misfit.

Figure 4 Comparison between synthetic PGV (computed with G83) (black) and PGV from ITA08 (grey) versus distance (km) for the magnitude classes 5.5, 6.0 and 6.5

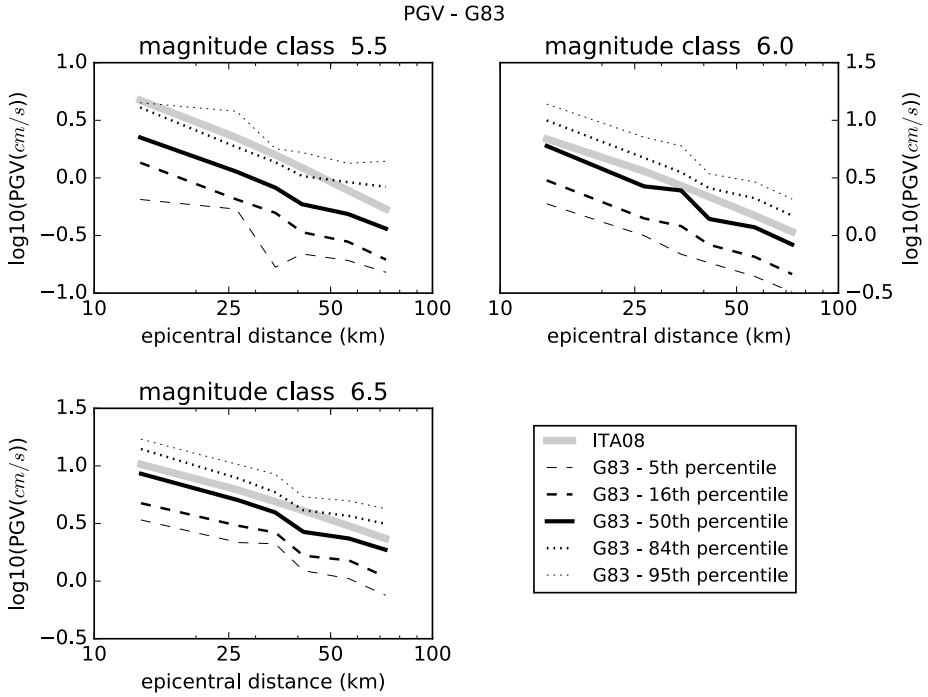

Note: The scatter of simulated PGV, reflected in the plot through quantile curves, results from the use of different focal mechanisms and different sites configurations.

The assessment of the uncertainty in the median of GMPE, due to the errors affecting the coefficients of the regression model, is crucial to ascertain if the obtained misfits are significant. For this purpose, we can use the results of Douglas (2007) who estimated the 95% confidence limits on the median PGA of seven models. He reported that, generally, for magnitudes in the range ($5.5 < M_W < 7$) and for epicentral distances in the range ($10 \leq R \leq 60$ km), the 95%-confidence limits of the median are narrow and are within the bands 10% to 30% from the median (0.04–0.11 in logarithmic unit), but become wider outside this limits. Therefore, we can consider misfits significant if their modulus is greater than 0.1.

4 Results of comparison of synthetic peaks computed using G83 with ITA08

The comparison between the synthetic peaks with G83 and those given by ITA08 (Figures 3 to 5) evidences the clear underestimation of simulated PGV for the lower magnitude classes (misfit is around –0.4 for $M = 5.0$ and –0.2 for $M = 5.5$). Simulated PGA is also underestimated for all magnitude classes (misfit between –0.1 and –1.2). The PGV misfit seems independent on distance, whereas PGA underestimation clearly increases with distance.

Figure 5 Misfit between ITA08 and simulated (a) PGV and (b) PGA (computed with G83 SLSS) for all magnitude classes, versus distance (km)

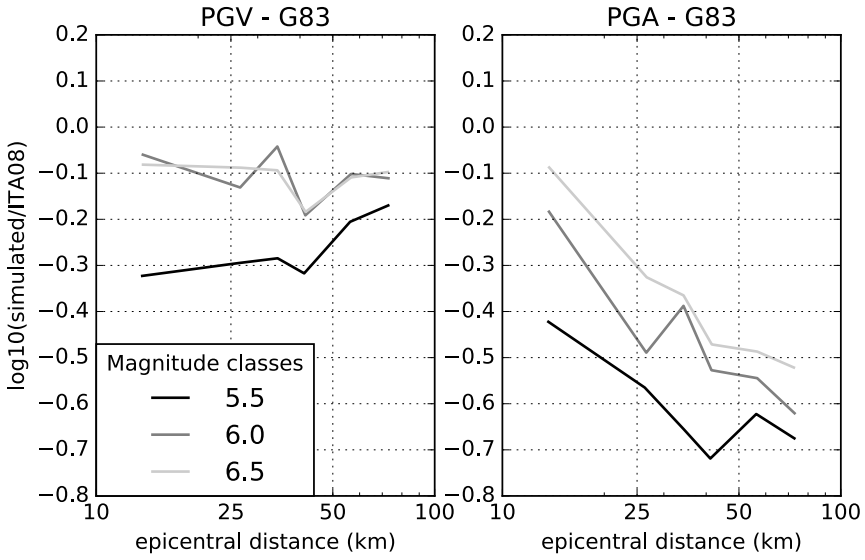

The observed misfits (see Figure 5) may have different origins. For example, the distribution in magnitude and the locations of the events that have been used for the NDSHA computation (see Figure 1) are often different from those of the events used in ITA08. If we compute the synthetic seismograms with the same earthquake sources used in the development of ITA08, many details of the distribution of peaks change, but the general trend of the misfits remains.

Naturally, the source depth has a great effect on peak values and some tests have been made to reduce the misfit between synthetic peaks and those of ITA08: for example, decreasing the source depth for low magnitude classes (e.g., 5 km for $M = 5.0$, instead of 10 km), the PGV misfit decreases, but there are not significant changes for PGA.

The different misfit of absolute levels for PGA and PGV suggests the necessity for a correction in the source spectral shape or for some structural parameters (i.e., Q) adjustment.

5 G83 scaling laws and their update

The revision of G83 relies on the studies of SLSS performed in the last decades. In order to clarify the lines of the necessary modification, it is useful to consider the key features of SLSS of G83, that either coincide or are different from the well-known scaling law proposed by Brune (1970) (henceforth named B70) (see Figure 6). The modified scaling law will be denoted G11D.

Figure 6 A sketch of two variants of SLSS: according to the standard ω^{-2} model (grey dashed lines), and according to the SLSS with two corner frequencies, each with a different kind of scaling (black solid lines)

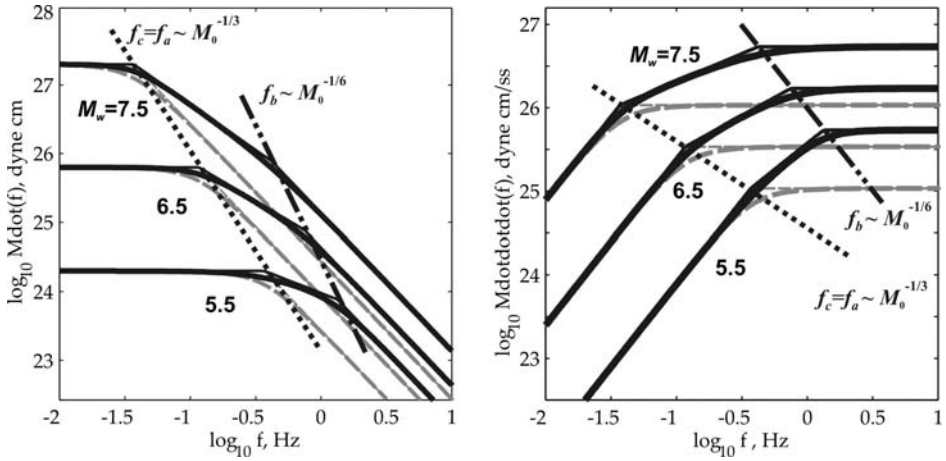

Notes: For each variant, the thicker line represents the expected spectrum and thin line its simplified version obtained combining line segments. The left panel represents $\dot{M}_0$ and the right panel shows 'acceleration' spectra $K(f) = \ddot{M}_0(f)$. Dotted and dash-dotted lines indicate trajectories of the first (f_a) and second (f_b) corner frequencies. For the standard ω^{-2} model, $f_C = f_a$.

5.1 G83 key features

1 *Scaling of corner frequency*. For spectra with a single corner frequency, its value is denoted f_C, while in the spectra with two corners (also if they may coincide) the lowermost corner is denoted f_{C1} and the second f_{C2}. It has been customary to calculate the corner frequency as $f_C^* = (f_{C1} \cdot f_{C2})$. However, it is f_{C1} that, at least in simple cases, is related to the inverse duration of the source time function, whereas f_C^* is mainly used in the definition of the 'spectral parameter' of Boore (2003) anchored at f_C^*; the use of f_C^* as a physical parameter can be misleading. In the construction of G83, the self-similar spectral scaling

$$f_{C1} \propto M_0^{-1/3} \tag{2}$$

where M_0 is the seismic moment, is assumed for the magnitude range 6.0–9.0. The assumed values of f_C are relatively low. If the popular B70 scaling law proposed by Brune (1970) is used:

$$f_C = 4.91\,10^6 V_S\,(\Delta\sigma / M_0)^{1/3} \text{ [km/s; dyne cm]} \tag{3}$$

where $\Delta\sigma$ is the stress drop, and V_S is the average S-wave crustal velocity, set at the popular value V_S = 3.5 km/s, then the scaling of f_{C1} in G83 corresponds to setting $\Delta\sigma \approx 13$ bar in equation (3). Both features – constant slope of 1/3 and its relatively low absolute level – should be preserved in the modified SLSS. The value of $\Delta\sigma$ in

equation (3) accepted in G11D is 15 bar. The reference magnitude used for the comparison of the parameters of SLSS is $M_W = 7$ ($\log_{10}M_0 = 26.55$). For G11D, the reference value is $f_{C1} = 0.062$ Hz for $M_W = 7$.

For lower magnitudes, a gradual decrease of stress drop, or, equivalently, a faster increase of f_{C1} with increasing M_0, was assumed in G83. So far, the question whether the stress drop decreases when passing from large earthquakes to moderate-to-small ones, or remains stable, is not resolved and is the subject of active debate. In any case, the degree of deviation from similarity (understood here as the case of $\Delta\sigma$ = constant) assumed in construction of G83 now looks extreme. There is no need to keep the feature of decreased stress drop at low M_W in the modified SLSS.

2 *Stable increase of high-frequency (HF) spectral level*. In G83, the HF spectral level A_{HF} (formally defined below) of SLSS increases, with increasing M_0, approximately following the scaling

$$A_{HF} \propto M_0^{1/3} \tag{4}$$

for $M_W \geq 6$. At lower magnitudes, the increase is faster, in agreement with the assumption of relatively lower $\Delta\sigma$ in equation (3). The relationship $\log_{10}A_{HF} = 1/3\log_{10}M_0 + const.$ follows from Brune (1970) or Aki (1967) SLSS. Since 1983, it has been confirmed in many studies, either directly for Japan (Irikura and Miyake, 2011) (following Dan et al., 2001; Morikawa and Fujiwara, 2003), or indirectly when fitting abundant Eastern North America (ENA) and Western USA (WUSA) acceleration data; still, the question is not settled completely, see below. Again, there is no need at present to assume significant deviations from the law equation (4) in the modified SLSS.

Boore (1986) has successfully checked the correctness of the absolute level of A_{HF} (M_0), predicted by G83. At present, average regional values of A_{HF} can be extracted from existing literature. For WUSA, the estimate of Atkinson and Silva (1997) can be converted to $\log_{10}A_{HF}(M_w = 7)$=26.22. For ENA, from Atkinson (1993) one can obtain $\log_{10}A_{HF}(M_w = 7) = 26.42$; the increase with respect to WUSA is a well-known feature of intraplate events. For Japan, the absolute level is $\log_{10}A_{HF}(M_w = 7) = 26.22$ after Irikura and Miyake (2011). However, many authors (Toro et al., 1997; Beresnev and Atkinson, 2002; Halldorsson and Papageorgiou, 2005) identified scaling behaviour of AHF that violates similarity. All of them found slower increase of A_{HF} vs. M_0 as compared to (4). Beresnev and Atkinson (2002), on the basis of mean trends derived from the WUSA dataset, found that the effective $\Delta\sigma$ for a point-source B70 model may drop from about 150 bars, for $M_w = 5$, to (extrapolated) 25 bars for $M_w = 8$. In other words, effective $\Delta\sigma$ or 'stress parameter' decreases with decreasing M_w. This apparently systematic feature could be easily assimilated into the revised SLSS, but we consider it premature to do it now.

3 *Two-corner shape and second corner frequency*. The characteristic feature of SLSS of G83 is a clear second corner or hump with specific corner frequency, denoted here f_{C2}. The SLSS with two corners was actually considered in the less popular section of the classic Brune (1970) paper and its origin was ascribed to fractional stress drop, but this possibility was not further investigated, probably because the problem of similarity of spectra (for various M_W) is not solved automatically, even if the reality

of two corners is taken as granted. The key point of G83 results is that f_{C2} trend slope is much smaller than that of f_{C1}. Therefore, no similarity exists for G83 spectra: spectral shapes for various magnitudes, plotted in log-log scale, are non-identical. No particular law for the actual behaviour of f_{C2} vs. f_{C1} or MW was proposed until Atkinson (1993) formulation for ENA: $\log_{10}(f_{C2}) = -0.188\, M_W + const$. Recently, the comparable trend

$$f_{C2} \propto M_0^{-1/6} \tag{5}$$

has been proposed for f_{C2} (Gusev, 2013), and it is followed here. The accepted reference value is $f_{C2}(M_W = 7) = 0.71$ Hz.

Values of stress drop of 25–30 bar are often reported as typical. In a large-scale study, fitting spectra of many thousands of world-wide shallow earthquakes, Allmann and Shearer (2009) recently determined average $\Delta\sigma \approx 30$ bar. On the other side, the characteristic value of the 'stress parameter', that defines A_{HF} and is closely related to f_{C2}, is typically estimated as 80–100 bar, or even greater. If one defines f_C as the geometric mean $f_C^* = (f_{C1} \cdot f_{C2})$, or, rather, fits the observed spectral shape with a single-corner ideal shape, the estimate of $\Delta\sigma$ related to f_C^*, $\Delta\sigma^*$, will also be close to the geometric mean of $\Delta\sigma(f_{C1})$ and $\Delta\sigma(f_{C2})$ (the latter being equivalent to 'stress parameter'). Setting $\Delta\sigma(f_{C2}) = 90$ bar and $\Delta\sigma^* = 30$ bar, one easily obtains $\Delta\sigma(f_{C1}) = 15$ bar, the value assumed above.

4 *Source-related* f_{max}. The G83 SLSS included a third corner frequency, in the range 5–10 Hz. Such a feature, or source-controlled f_{max}, was proposed by Papageorgiou and Aki (1983). The f_{max} as defined in SLSS of G83 requires a radical revision. As proposed by Anderson and Hough (1984), the f_{max} observed in acceleration spectra (after their correction for path-related attenuation) is caused by significant near-receiver (site-related) attenuation, either completely or to a significant degree. However, in many cases, the source-related contribution to formation of 'f_{max} cut-off' can be revealed; see Gusev (2013) for a short review. Typically, the source-controlled f_{max}, when observable, is above 5 Hz. This part of the spectrum is less relevant for hazard calculations, and, in a first approximation, the effect of source-related f_{max} on spectra can be ignored. Thus, for frequencies above f_{C2}, all acceleration spectra will be assumed flat, since it is easy to account for f_{max}, in the range 7–20 Hz, if needed.

5.2 G11D: the new scaling law

The SLSS of G83 is semi-empirical by construction, and is given in graphical form. To represent SLSS by means of an analytical expression has many advantages. We shall use the expression (Atkinson, 1993):

$$m(f) = \frac{M_0(f)}{M_0}\left[\left(\frac{1-\varepsilon}{1+(f/f_{C1})}\right)+\left(\frac{\varepsilon}{1+(f/f_{C2})^2}\right)\right]$$

i.e., a sum of two simple Brune's (1970) spectra with two corner frequencies f_{C1} and $f_{C2} > f_{C1}$, providing the f^{-2} HF asymptote (see Figure 6). This choice permits to emulate

spectral humps if needed; e.g., to reproduce the two-humped spectra of G83. The lower corner frequency f_{C1} is related to fault dimensions or rupture duration, whereas the physical meaning of the second corner frequency f_{C2} is not so clear. Papageorgiou and Aki (1983) and later Beresnev and Atkinson (2002) relate f_{C2} to the characteristic size of an assumed crack-like subsource, whereas Gusev (2013) believes that it is related to the local rise time, T_R, and to the slip-pulse width l.

In the following, the main notion is the *rms* average acceleration source spectrum $K(f) \equiv |\ddot{M}_0(f)| = |(2\pi f)^2 \dot{M}_0(f)|$ of an equivalent point source whose displacement STF is

$$\dot{M}_0(t) = FT^{-1}\left(\dot{M}_0(f)\right)$$

It can be described, on the basis of the selected displacement spectral shape, as

$$K(f) = (2\pi f)^2 M_0 \left((1-\varepsilon)\left(1+\frac{f^2}{f_{C1}^2}\right)^{-1} + \varepsilon\left(1+\frac{f^2}{f_{C2}^2}\right)^{-1} \right) \tag{6}$$

Two reference values of $K(f)$ are introduced. The first one is A_{LF}

$$A_{LF} = \left(2\pi f_{C1}\right)^2 M_0 \tag{7}$$

A_{LF} mostly defines the spectral behaviour around $f = f_{C1}$. It expresses the lowermost HF asymptotic acceleration spectral level at the given (M_0, f_{C1}) combination, attained at $\varepsilon = 0$, when the spectral shape follows one-corner spectrum of the Brune (1970) shape with $f_C = f_{C1}$. Another reference parameter is the actual HF asymptotic acceleration spectral level

$$A_{HF} = K\left(f\big|_{f\to\infty}\right) = (2\pi)^2 M_0 \left((1-\varepsilon) f_{C1}^2 + \varepsilon f_{C2}^2\right) \tag{8}$$

The ε parameter ($0 < \varepsilon < 1$) in equation (6) can be expressed through the ratio $K = A_{HF} / A_{LF}$ as

$$\varepsilon = (K-1) \Big/ \left(\left(f_{C1}/f_{C2}\right)^2 - 1 \right) \tag{9}$$

Again following Atkinson (1993), the existence of approximate linear trends between M_W and logarithms of f_{C1}, f_{C2} and A_{HF} is assumed.

Having set the value of M_0, and determining f_{C1}, f_{C2}, and A_{HF} from empirical trends, it is possible to define the characteristic or reference spectral shape in a broad frequency band and generate the desired SLSS. The value of the dependent parameter, ε, is determined from equation (9), with $A_{LF} = A_{LF}(M_0, f_{C1})$.

To determine f_{C1}, one can apply equation (3): using the values V_S = 3.5 km/s and $\Delta\sigma$ = 15 bar the reference value f_{C1} = 0.06 at M_W = 7 is determined. f_{C2} can be determined from

$$\log_{10} f_{C2} = -0.15 + 0.25(7 - M_W) \tag{10}$$

which implements the scaling of equation (5) and gives the reference value 0.7 Hz at M_W = 7. To determine A_{HF}, the formula of Irikura-Dan-Morikawa (Irikura and Miyake, 2011; Dan et al., 2001; Morikawa and Fujiwara, 2003) is used:

$$\log_{10} A_{HF} = 25.03 + (1/3)\left(\log_{10} M_0 - 23\right) \tag{11}$$

This A_{HF} level is reproduced by B70 spectrum equation (3) at $\Delta\sigma$ = 87.5 bar. In Figure 7, the obtained spectral family (named G11D) is shown for M_W = 4.5, 5.5, 6.5, 7.5 and 8.5, respectively. For reference, B70 spectra for 15 and 87.5 bar, and the G83 spectral family are given. Additional reference points at f = 0.05 Hz (20 s) are derived from the M_S(*USNEIC*) vs. M_0 trend. This trend is based on the M_S(*GR*) trend compiled by Gusev (1991), with slight correction.

Figure 7 SLSS families are shown as $K(f)$ functions in units of dyne cm/s^2

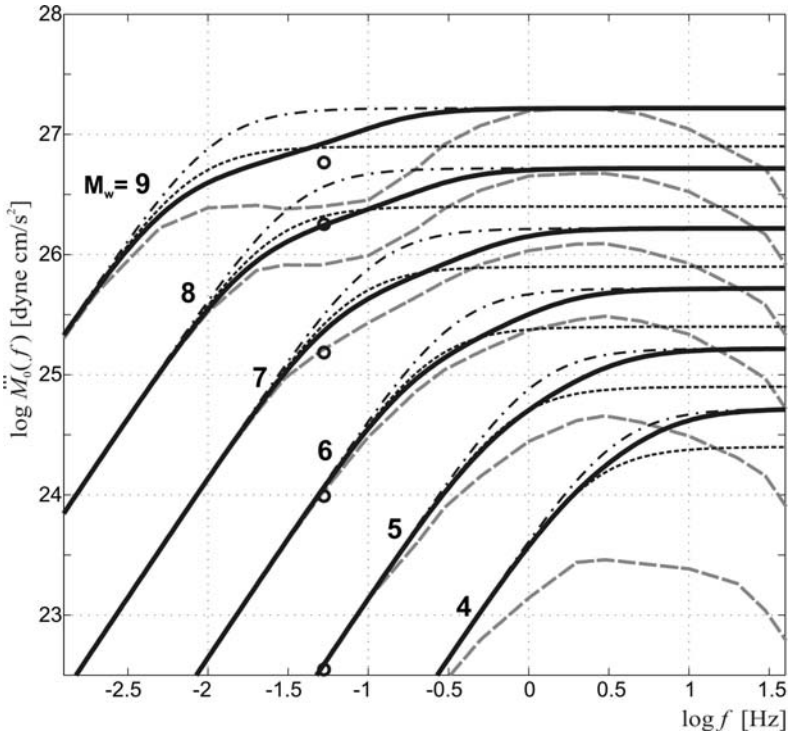

Notes: Solid lines: proposed SLSS denoted 'G11D' for magnitudes in the range 4–9; dash-doted and dashed lines: SLSS after B70 for $\Delta\sigma$ = 15 bar and 87.5 bar, respectively; grey dashed lines: SLSS of G83. Abscissa: $\log_{10}(f, Hz)$. Ordinate: $\log_{10}(K(f))$. Small circles: values of $K(f$ = 0.05 Hz) at selected magnitudes derived from the empirical M_S vs. M_W trend of Gusev (1991).

5.3 Comparison of G11D with ITA08

When applied to strong motion synthesis, the G11D spectral family gives acceptable results for PGV (see Figures 8 and 10). The misfits for the different magnitudes seem independent on distance and for magnitude 5.5, 6.0 and 6.5 are limited between –0.1 and 0.1. For magnitude 5.0, the underestimation is between –0.1 and –0.4, but with G83 spectral family the misfit for magnitude 5.0 was much larger, between –0.3 and –0.7.

Figure 8 Comparison between synthetic PGV (computed with G11D) (black) and PGV from ITA08 (grey) versus distance (km) for the magnitude classes 5.5, 6.0 and 6.5

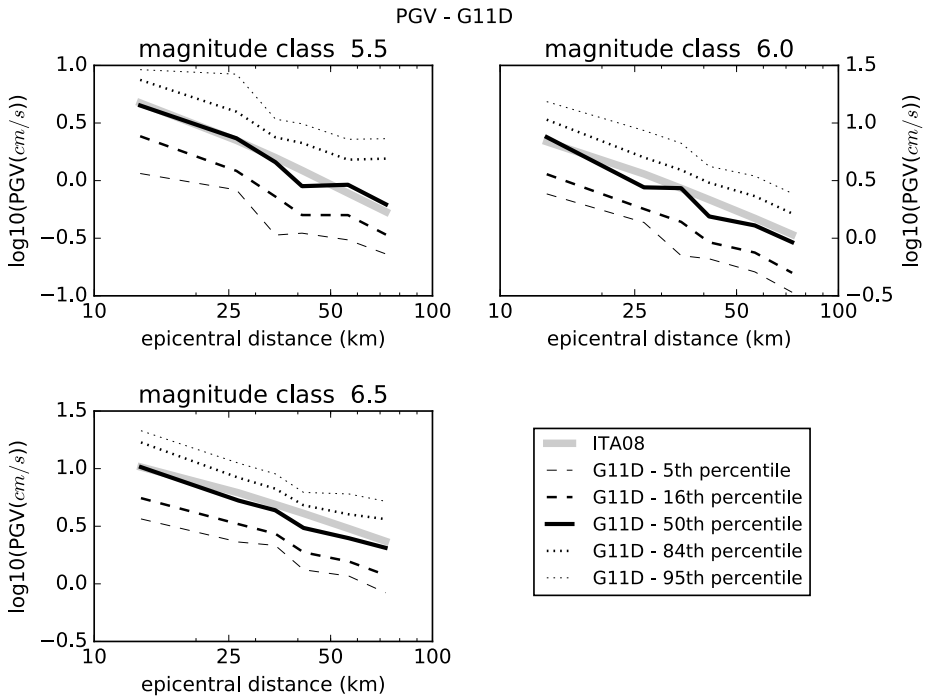

Note: The scatter of simulated PGV, reflected in the plot through quantile curves, results from the use of different focal mechanisms and different sites configurations.

When acceleration is considered the comparison is not good (see Figures 9 and 10). The different magnitude classes show a similar behaviour: the agreement with ITA08 is good at short distances (misfit between –0.2 and 0.0), but then synthetic PGA attenuates faster than ITA08 ones (at 100 km of distance the misfit is around –0.6). A simple change in the attenuation model can drastically improve the correspondence between NDSHA modelling and ITA08 peak values. In fact, doubling the Q (quality factor) values for all Italian cellular structures the attenuation with distance of synthetic PGA becomes similar to that of ITA08 (see Figure 11) and this variation is consistent with the uncertainties affecting Q measurements (Craglietto et al., 1989; Martínez et al., 2010).

Massa et al. (2012), who compared ITA08 and other GMPE to ground motion data from L'Aquila sequence, show that all models they considered, especially at high and intermediate (1.0 Hz) frequencies, predict ground motion larger than that observed during the L'Aquila sequence. The overshooting of the predictions by ITA08, observed for epicentral distances greater than 10 km, could be partially justified by the absence of the anelastic attenuation coefficient in the functional form of the considered GMPE. A direct comparison between the observed and simulated peaks overcomes the dependence from the functional form of used GMPE, therefore, the NDSHA peaks are directly compared with the pertinent set of observed peaks.

Figure 9 Comparison between synthetic PGA (computed with G11D) (black) and PGA from ITA08 (grey) versus distance (km) for the magnitude classes 5.5, 6.0 and 6.5

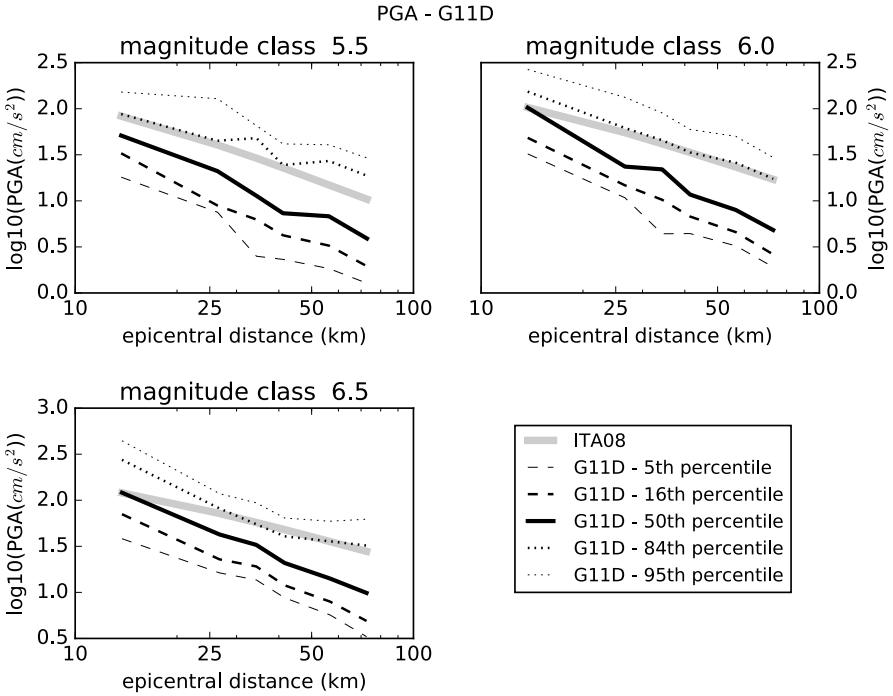

Note: The scatter of simulated PGA, reflected in the plot through quantile curves, results from the use of different focal mechanisms and different sites configurations.

Figure 10 Misfit between ITA08 and simulated (a) PGV and (b) PGA (computed with G11D SLSS) for all magnitude classes, versus distance (km)

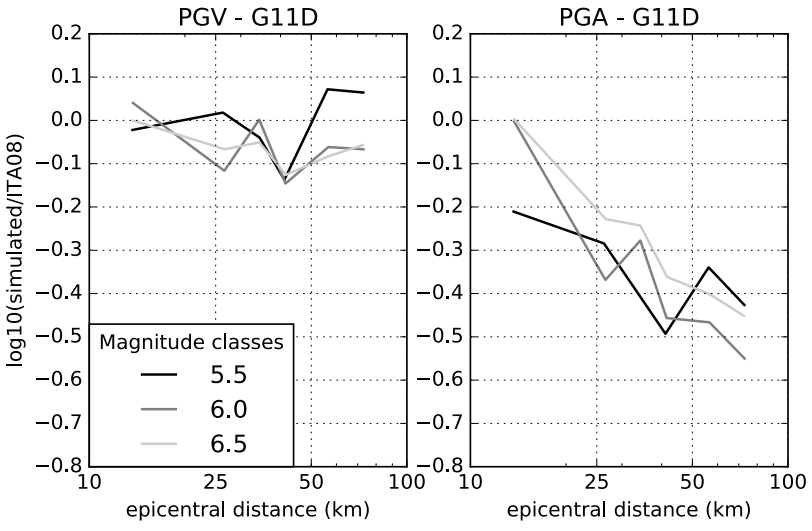

(a) (b)

Figure 11 Misfit between ITA08 and simulated PGA (computed with G11D SLSS) for all magnitude classes 5.5, 6.0 and 6.5

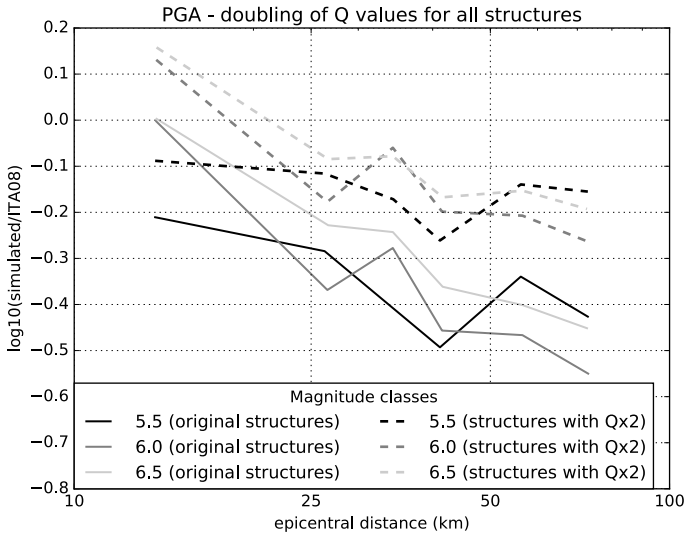

Notes: Solid lines show the results obtained with the cellular models by Brandmayr et al. (2010); dashed lines show the results obtained simply doubling the Q values in the same cellular models.

6 Comparison with observed ground motions

The values extracted from our synthetic signals, that are obtained using the same source and structural parameters adopted at national scale for NDSHA, are compared with the values empirically observed as a consequence of real earthquakes.

The recorded signals are taken from ITACA (Luzi et al., 2008) and from the website RAN Download of the Italian Civil Protection Department – Presidency of the Council of Ministers (http://ran.protezionecivile.it/IT/index.php). Only the signals from events with magnitude $M_W \geq 5.0$, and depth < 50 km, recorded at stations classified as A (or A*) EC8 soil class with an epicentral distance ≤ 250 km are considered. The events selected are listed in Table 1: most of them belong to Umbria-Marche (1997 to 1998), L'Aquila (2009) and Emilia (2012) sequences. ITA08 was calibrated with events up to 2007: therefore, L'Aquila (2009) and Emilia (2012) sequences have obviously not been used for the calibration and, therefore, supply a useful set of observation that can be used for a reliable test. Figure 12 shows the histogram of the number of seismograms grouped accordingly to epicentral distances and magnitudes classes.

Figure 12 Number of seismograms divided in classes of (a) epicentral distances and (b) of magnitudes

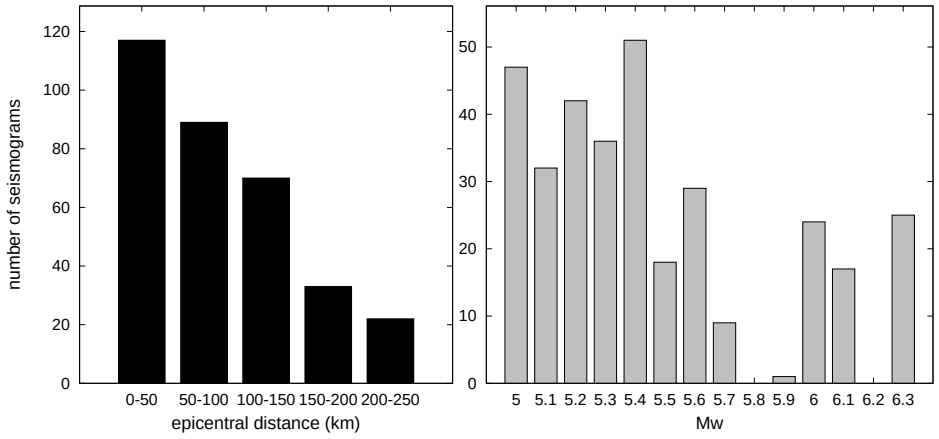

(a) (b)

Figure 13 (a) Focal mechanisms of the events listed in Table 1 and boundaries of the seismogenic zones of ZS9 (Meletti et al., 2008) in grey (b) Geographic distribution of the recording stations and boundaries of the cellular models (Brandmayr et al., 2010) in grey

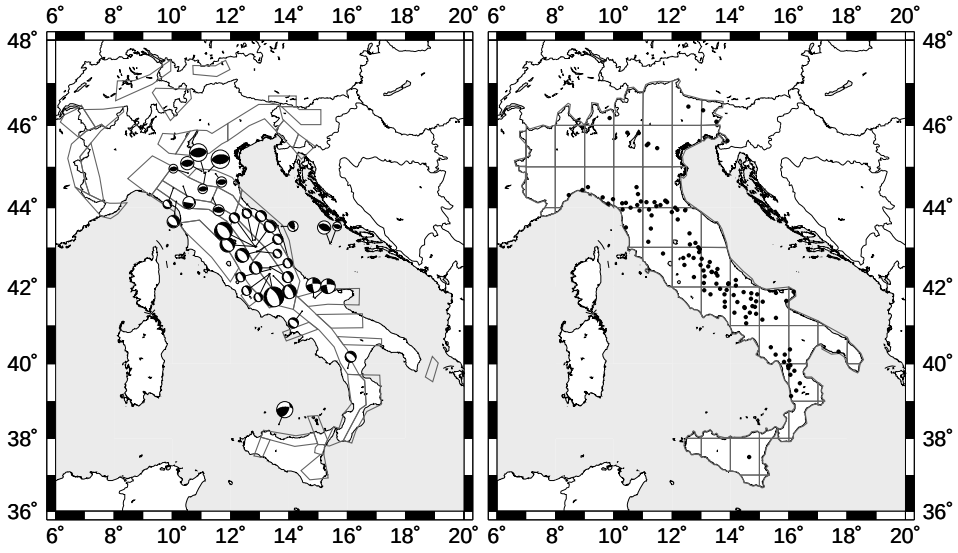

(a) (b)

Table 1 Events selected for the comparison between synthetic (NDSHA) and observed peaks

Date	*Time*	*Lat (°)*	*Lon (°)*	*M*	h_o *(km)*
26/09/1997	00:33:12	43.023	12.891	5.7	3.5
26/09/1997	09:40:25	43.015	12.854	6.0	9.9
03/10/1997	08:55:22	43.043	12.824	5.2	12.1
06/10/1997	23:24:53	43.028	12.847	5.4	3.9
12/10/1997	11:08:36	42.906	12.920	5.2	0.1
14/10/1997	15:23:09	42.898	12.899	5.6	7.3
21/03/1998	16:45:09	42.900	12.900	5.0	1.1
26/03/1998	16:26:17	43.190	12.840	5.3	44.8
03/04/1998	07:26:36	43.185	12.757	5.1	1.9
06/09/2002	01:21:29	38.381	13.654	5.9	27.0
31/10/2002	10:32:59	41.717	14.893	5.7	25.2
01/11/2002	15:09:02	41.742	14.843	5.7	21.4
29/03/2003	17:42:16	43.101	15.413	5.5	21.7
14/09/2003	21:42:53	44.230	11.387	5.3	15.8
25/11/2004	06:21:17	43.135	15.446	5.0	10.0
23/12/2008	15:24:21	44.519	10.382	5.4	26.7
06/04/2009	01:32:39	42.334	13.334	6.3	8.8
06/04/2009	02:37:04	42.336	13.340	5.1	10.1
06/04/2009	23:15:37	42.451	13.364	5.1	8.6
07/04/2009	09:26:28	42.336	13.340	5.0	10.2
07/04/2009	17:47:37	42.275	13.464	5.6	15.1
09/04/2009	00:52:59	42.484	13.343	5.4	15.4
09/04/2009	19:38:16	42.501	13.356	5.3	17.2
13/04/2009	21:14:24	42.504	13.363	5.1	7.5
25/01/2012	08:06:37	44.85	10.54	5.0	33.0
27/01/2012	14:53:14	44.48	10.03	5.0	50.0
20/05/2012	02:03:53	44.89	11.25	6.1	10.00
20/05/2012	03:02:50	44.86	11.15	5.1	10.00
20/05/2012	13:18:00	44.83	11.49	5.2	15.00
29/05/2012	07:00:00	44.85	11.09	6.0	15.00
29/05/2012	10:55:57	44.89	11.01	5.5	6.80
25/10/2012	23:05:24	39.88	16.01	5.3	15.00
21/06/2013	10:33:57	44.15	10.14	5.4	5.10
21/07/2013	01:32:24	43.53	13.74	5.2	10.00
29/12/2013	17:08:43	41.37	14.45	5.2	11.00

For each event, a ground motion scenario is computed by the NDSHA modelling technique, with the same assumptions (i.e., source and structural parameters) adopted when performing the comparison with ITA08. The only difference is that here the geographical locations of sources [see Figure 13(a)], taken from the RCMT catalogue (Pondrelli et al., 2006, 2009) and stations [see Figure 13(b)] are used, instead of regular grids of sources and receivers, as in the comparisons of Section 3. For the events that fall outside of the seismogenic zones, the focal mechanisms are taken from the RCMT catalogue. The observed and synthetic seismograms have been filtered with a Gaussian low pass filter with a cut-off frequency of 10 Hz, the same used in the modelling.

6.1 Comparison of observed and synthetic parameters

As for the test against GMPE, we consider the largest horizontal component between the north-south and east-west. We compare the PGV, PGA and SAs (at 0.1, 0.2, 0.5, 1, 2 and 3 s) extracted from the NDSHA (synthetic) and observed seismograms. Residuals, ε, are defined as: $\varepsilon = \log_{10}(y_{syn} / y_{obs})$, where y_{obs} is the observed peak value and y_{syn} is the corresponding synthetic peak value.

In the first variant of the computations, the source functions computed with G83 are used. Figure 14 shows the obtained residuals versus epicentral distance and Table 2 gives the mean and standard deviations of the residuals for this set of data. The synthetic seismograms underestimate PGA, PGV and SAs at periods shorter than 1 s. The mean residual for PGA is –0.44, which corresponds to a ratio 0.36. PGV from the synthetic signals are closer to observations: the mean residual is –0.17, which corresponds to a ratio 0.67. In the second variant G11D is used: the mean residuals are nearer to zero (for example: –0.12 for PGA and 0.07 for PGV) (see Table 2 and Figure 15) and the median value of residuals (grey lines in Figure 15) decreases with increasing distance. For both tests, the values of standard deviation of the residuals are similar to the results reported in Douglas et al. (2004) for similar tests. The uncertainty in synthetic peak values due to uncertainties about earthquake location (as reported by the RCMT catalogue) and magnitude (Gasperini et al., 2012) is negligible with respect to the standard deviation of residuals (as shown in Figures 14 and 15).

Table 2 Mean (μ) and standard deviation (σ) of residuals of the horizontal peaks and SA for the computations with G83 and G11D SLSS (Section 3.1) and for the two parametric tests described in Section 3.2

	G83		*G11d*		*G11d + RCMT*		*G11d + RCMT + depth*	
	μ	σ	μ	σ	μ	σ	μ	σ
ε(PGA)	–0.43 ± 0.03	0.48	–0.11 ± 0.03	0.55	–0.12 ± 0.03	0.56	–0.16 ± 0.03	0.62
ε(PGV)	–0.19 ± 0.02	0.39	0.03 ± 0.02	0.43	0.03 ± 0.02	0.42	–0.00 ± 0.03	0.50
ε(SA(0.1))	–0.65 ± 0.03	0.48	–0.19 ± 0.03	0.57	–0.20 ± 0.03	0.58	–0.23 ± 0.04	0.64
ε(SA(0.2))	–0.66 ± 0.03	0.57	–0.28 ± 0.04	0.66	–0.30 ± 0.04	0.66	–0.31 ± 0.04	0.71
ε(SA(0.5))	–0.36 ± 0.03	0.52	–0.04 ± 0.03	0.57	–0.05 ± 0.03	0.57	–0.08 ± 0.04	0.63
ε(SA(1.0))	0.08 ± 0.03	0.46	–0.01 ± 0.03	0.46	–0.02 ± 0.03	0.45	–0.06 ± 0.03	0.53
ε(SA(2.0))	0.07 ± 0.02	0.37	0.04 ± 0.02	0.36	0.02 ± 0.02	0.37	–0.00 ± 0.03	0.46
ε(SA(3.0))	0.04 ± 0.02	0.35	0.11 ± 0.02	0.36	0.10 ± 0.02	0.37	0.08 ± 0.02	0.43

Note: For each mean value is reported the confidence interval at 1σ.

Figure 14 PGA, PGV and horizontal SA residuals ($\varepsilon = \log_{10}(y_{syn} / y_{obs})$) versus epicentral distance

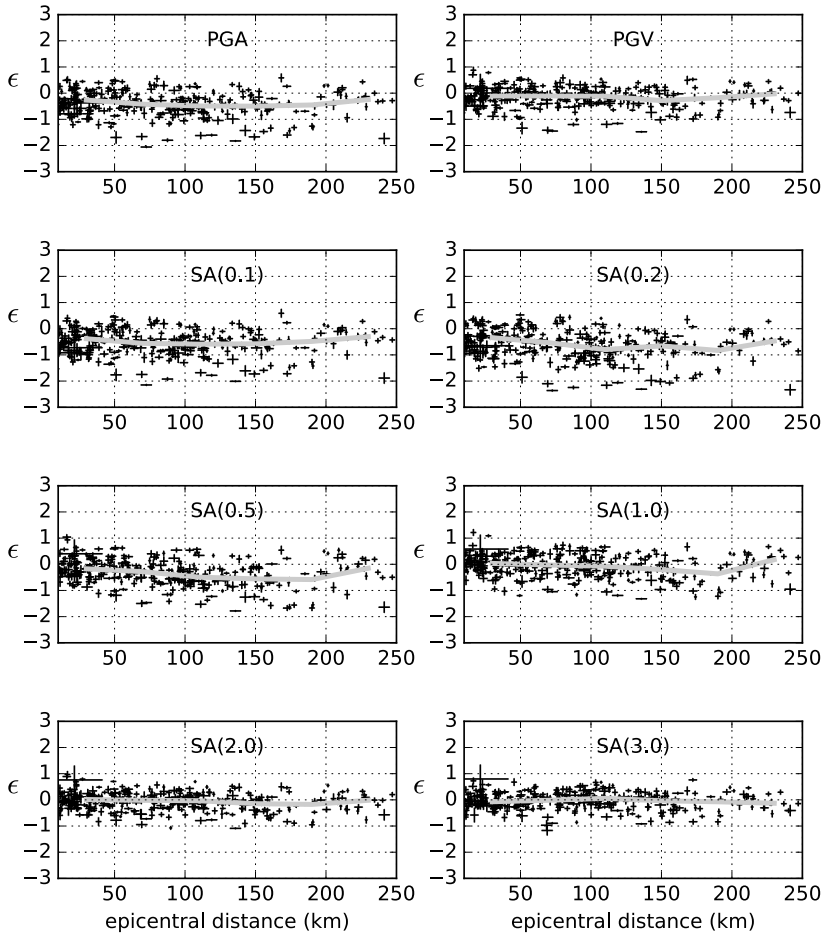

Notes: Synthetic signals are computed with NDSHA procedure using the cellular structures and G83. The grey lines show the medians of residuals. Error bars on the y-axis represent uncertainties in modelling due to uncertainties in input parameters (earthquake location and magnitude).

6.2 Parametric tests

The influence of different parameters of the earthquake source (i.e., focal mechanism and depth) on the distribution of residuals has been tested considering the RCMT catalogue (Pondrelli et al., 2006, 2009) instead of the focal mechanisms associated with each seismogenic zone [Figure 13(a)]. From Table 2, it is evident that the mean residuals (G11D + RCMT in Table 2) are not affected by the change. Similarly, for depths up to 25 km, the difference between the depth (10 km) adopted in NDSHA calculations (h_{NDSHA}) and the observed depth (h_0), listed in Table 1, does not affect the residuals. This

fact can be naturally explained considering that the uncertainties in h_0 are comparable with the difference between h_0 itself and h_{NDSHA}, even if some contribution from other uncertainties in the modelling may mask this dependence. For completeness, we report that for the few events with $h_0 \geq 25$ km, NDSHA peaks underestimate the observed ones but the quantity of available data does not allow, at the moment, any further investigation.

Figure 15 PGA, PGV and horizontal SA residuals ($\varepsilon = \log_{10}(y_{syn} / y_{obs})$) versus epicentral distance

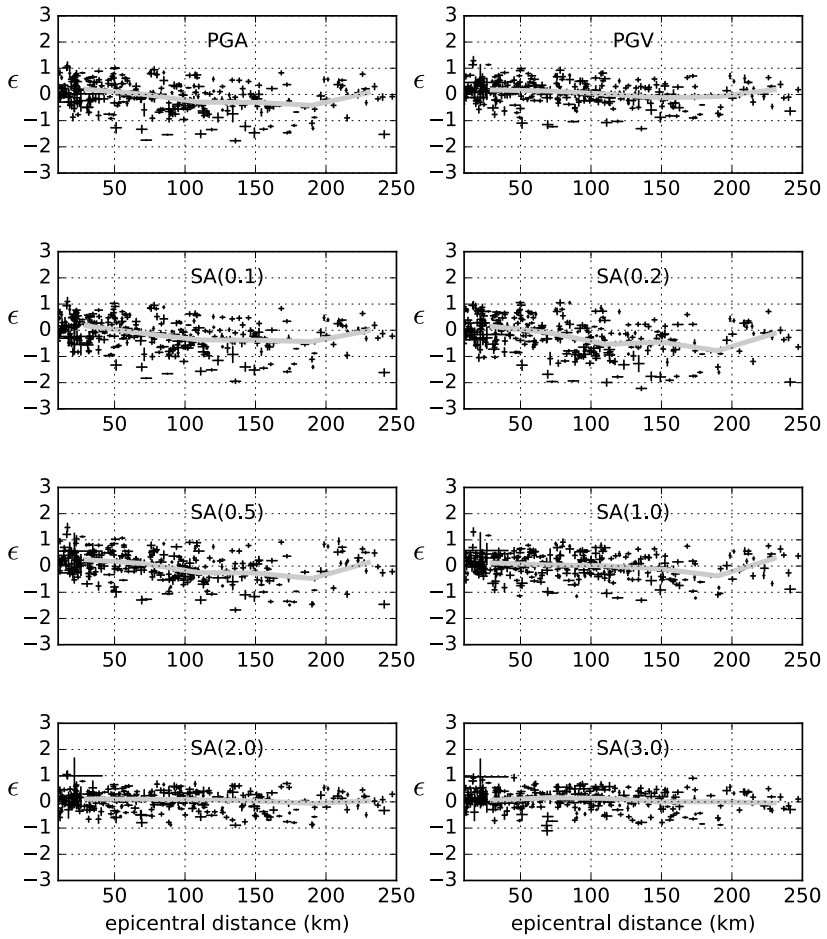

Notes: Synthetic signals are computed with NDSHA procedure using the cellular structures and G11D. The grey lines show the medians of residuals. Error bars on the y-axis represent uncertainties in modelling due to uncertainties in input parameters (earthquake location and magnitude).

As evidenced in the comparison with GMPEs, the dependence of residuals on epicentral distance (especially for PGA and SA at short periods) suggests that the quality factors Q_S and Q_P given in the cellular models by Brandmayr et al. (2010) are systematically too low.

7 Conclusions

The results of national scale NDSHA modelling for the Italian region at 10 Hz cut-off are compared with ITA08 empirical attenuation relations and with instrumental observations considering peak ground motion values (PGV and PGA) and SA.

The new set of source spectra, defined along the lines suggested by the comparison with ITA08, produces acceptable results in terms of PGV and SA at long periods. Synthetic PGA and SA at short periods show a faster attenuation with respect to the observed ones and to ITA08. Reasonable variations of the focal mechanism and source depth, with respect to those used in NDSHA, have limited effects on residuals scatter and average.

Even if a simple doubling of the Q values in the uppermost part of the models seems to lead to acceptable misfits with respect to ITA08, the influence of anelasticity has to be explored more in detail, in future ad hoc studies. Smaller misfits at long periods than at short ones are congruent with the resolution of the available structural models, obtained from the inversion of surface wave dispersion curves at periods longer than 5 s, and evidence the opportunity to improve the resolution of the uppermost part of the model analysing shorter period surface waves, that are responsible of most of the impact observed as a consequence of damaging earthquakes.

The comparison of ground motion parameters at long period derived by synthetic seismograms (NDSHA) with GMPE is an interesting topic from the practical and theoretical point of view. From surface waves theory, the displacement of the fundamental mode dominates the earthquake ground motion at long period, $T \geq 5$ s (Panza et al., 1973, 1975a, 1975b), therefore, the separation of the propagation from the source contribution to earthquake ground motion, commonly, but incorrectly, assumed in GMPE, is possible without relevant violation of the tensor nature of earthquake ground motion. The prediction of ground motion at long period is a crucial requirement by displacement-based design techniques. Even if there are empirical models for PGD and for displacement response spectra that used data also from Italy (e.g., Campbell and Bozorgnia, 2008; Cauzzi et al., 2015), empirical models specific for the Italian region are not available. Therefore, the results obtained by NDSHA are, at present, the only existing reliable and physically rooted estimates of PGD for this area. PGD supplied by NDSHA is reliable since it is obtained by straightforward analytical (not numerical) integration, with respect to time, of the signals used to extract PGV or PGA, supplied by NDSHA, whose misfit with observations has been described in detail in Section 6.

The use of the STSPS representation of the source introduces a stochastic element in NDSHA that allows for the generation of a set of earthquake ground motions that encompass the possible variability in shaking at a site from a given event. A possible design strategy based on the definition of seismic input as described in this work is given by Fasan et al. (2015), where comparisons with examples of spectral shapes from Italian Building Code (NTC08, 2008) are shown and discussed, and in Fasan et al. (2017) where the entanglement of near source and site effects is treated.

Acknowledgements

Some of the results shown in this work have been obtained within the framework of International and National agreements. In particular, we acknowledge the partial support of the Veneto Regional Secretariat of the Italian Ministry of Cultural Heritage and Activities and Tourism (MiBACT). The partial support by the grant from the Russian Science Foundation (project #14-17-00621) is acknowledged for the section regarding the development of the new SLSS.

References

Aki, K. (1967) 'Scaling law of seismic spectrum', *Journal of Geophysical Research*, Vol. 72, No. 4, pp.1217–1231.

Aki, K. (1987) 'Strong motion seismology', in Erdik, M.Ö. and Toksöz, M.N. (Eds.): *Strong Ground Motion Seismology*, No. 204 in NATO ASI Series, Series C: Mathematical and Physical Sciences, Springer.

Allmann, B.P. and Shearer, P.M. (2009) 'Global variations of stress drop for moderate to large earthquakes', *J. Geophys. Res.*, Vol. 114, B01310, doi:10.1029/2008JB005821.

Anderson, D.L. (2007) *New Theory of the Earth*, Cambridge University Press, New York.

Anderson, J.G. and Hough, S.E. (1984) 'A model for the shape of the Fourier amplitude spectrum of acceleration at high frequencies', *Bulletin of the Seismological Society of America*, Vol. 74, No. 5, pp.1969–1993.

Atkinson, G.M. (1993) 'Earthquake source spectra in Eastern North America', *Bulletin of the Seismological Society of America*, Vol. 83, No. 6, pp.1778–1798.

Atkinson, G.M. and Silva, W. (1997) 'An empirical study of earthquake source spectra for California earthquakes', *Bulletin of the Seismological Society of America*, Vol. 87, No. 1, pp.97–113.

Beresnev, I.A. and Atkinson, G.M. (2002) 'Source parameters of earthquakes in eastern and western North America based on finite-fault modeling', *Bulletin of the Seismological Society of America*, Vol. 92, No. 2, pp.695–710.

Bindi, D., Luzi, L., Massa, M. and Pacor, F. (2010) 'Horizontal and vertical ground motion prediction equations derived from the ITalian Accelerometric Archive (ITACA)', *Bulletin of Earthquake Engineering*, Vol. 8, No. 5, pp.1209–1230.

Boore, D.M. (1986) 'The effect of finite bandwidth on seismic scaling relationships', in S. Das, J. Boatwright and C.H. Scholz (Eds.): *Earthquake Source Mechanics*, pp.275–283, doi: 10.1029/GM037p0275, American Geophysical Union, Washington, DC.

Boore, D.M. (2003) 'Simulation of ground motion using the stochastic method', *Pure and Applied Geophysics*, Vol. 160, Nos. 3–4, pp.635–676.

Brandmayr, E., Raykova, R.B., Zuri, M., Romanelli, F., Doglioni, C. and Panza, G.F. (2010) 'The lithosphere in Italy: structure and seismicity', *Journal of the Virtual Explorer*, Vol. 36, DOI; 10.3809/jvirtex.2009.00224.

Brune, J.N. (1970) 'Tectonic stress and the spectra of seismic shear waves from earthquakes', *Journal of Geophysical Research*, Vol. 75, No. 26, pp.4997–5009.

Campbell, K.W. and Bozorgnia, Y. (2008) 'NGA ground motion model for the geometric mean horizontal component of PGA, PGV, PGD and 5% damped linear elastic response spectra for periods ranging from 0.01 to 10 s', *Earthquake Spectra*, Vol. 24, No. 1, pp.139–171.

Cauzzi, C., Faccioli, E., Vanini, M. and Bianchini, A. (2015) 'Updated predictive equations for broadband (0.01–10 s) horizontal response spectra and peak ground motions, based on a global dataset of digital acceleration records', *Bulletin of Earthquake Engineering*, Vol. 13, No. 6, pp.1587–1612.

Cosenza, E. and Manfredi, G. (2000) 'Damage indices and damage measures', *Progress in Structural Engineering and Materials*, Vol. 2, No. 1, pp.50–59.

CPTI Working Group (2004) *Catalogo Parametrico dei Terremoti Italiani*, INGV, Bologna [online] http://emidius.mi.ingv.it/CPTI.

Craglietto, A., Panza, G.F., Mitchell, B.J. and Costa, G. (1989) 'Anelastic properties of the crust in the Mediterranean area', in *American Geophysical Union Geophysical Monograph*, Vol. 6, pp.179–196, Wiley Online Library.

Dan, K., Watanabe, M., Sato, T. and Ishii, T. (2001) 'Short-period source spectra inferred from variable-slip rupture models and modeling of earthquake faults for strong motion prediction by semi-empirical method', *Journal of Structural and Construction Engineering*, Vol. 545, pp.51–62.

Decanini, L.D. and Mollaioli, F. (1998) 'Formulation of elastic earthquake input energy spectra', *Earthquake Engineering & Structural Dynamics*, Vol. 27, No. 12, pp.1503–1522.

Douglas, J. (2007) 'On the regional dependence of earthquake response spectra', *ISET Journal of Earthquake Technology*, Vol. 44, No. 1, pp.71–99.

Douglas, J., Suhadolc, P. and Costa, G. (2004) 'On the incorporation of the effect of crustal structure into empirical strong ground motion estimation', *Bulletin of Earthquake Engineering*, Vol. 2, No. 1, pp.75–99.

Fasan, M., Amadio, C., Noè, S., Panza, G.F., Magrin, A., Romanelli, F. and Vaccari, F. (2015) 'A new design strategy based on a deterministic definition of the seismic input to overcome the limits of design procedures based on probabilistic approaches', in *XVI ANIDIS Conference*, L'Aquila, Italy.

Fasan, M., Magrin, A., Amadio, C., Panza, G.F., Romanelli, F., Vaccari, F. and Noè, S. (2017) 'A possible revision of the current seismic design process to overcome the limitations of standard probabilistic seismic input definition', in *16th World Conference on Earthquake, 16WCEE 2017*, Santiago Chile.

Gasperini, P., Lolli, B., Vannucci, G. and Boschi, E. (2012) 'A comparison of moment magnitude estimates for the European-Mediterranean and Italian regions', *Geophysical Journal International*, Vol. 190, No. 3, pp.1733–1745.

Gusev, A.A. (1983) 'Descriptive statistical model of earthquake source radiation and its application to an estimation of short-period strong motion', *Geophysical Journal of the Royal Astronomical Society*, Vol. 74, No. 3, pp.787–808.

Gusev, A.A. (1991) 'Intermagnitude relationships and asperity statistics', *Pure and Applied Geophysics*, Vol. 136, No. 4, pp.515–527.

Gusev, A.A. (2011) 'Broadband kinematic stochastic simulation of an earthquake source: a refined procedure for application in seismic hazard studies', *Pure and Applied Geophysics*, Vol. 168, No. 1, pp.155–200.

Gusev, A.A. (2013) 'High-frequency radiation from an earthquake fault: a review and a hypothesis of fractal rupture front geometry', *Pure and Applied Geophysics*, Vol. 170, Nos. 1–2, pp.65–93.

Halldorsson, B. and Papageorgiou, A.S. (2005) 'Calibration of the specific barrier model to earthquakes of different tectonic regions', *Bulletin of the Seismological Society of America*, Vol. 95, No. 4, pp.1276–1300.

Irikura, K. and Miyake, H. (2011) 'Recipe for predicting strong ground motion from crustal earthquake scenarios', *Pure and Applied Geophysics*, Vol. 168, Nos. 1–2, pp.85–104.

Luzi, L., Hailemikael, S., Bindi, D., Pacor, F., Mele, F. and Sabetta, F. (2008) 'ITACA (ITalian ACcelerometric Archive): a web portal for the dissemination of Italian strong-motion data', *Seismological Research Letters*, Vol. 79, No. 5, pp.716–722.

Martínez, M.D., Lana, X. and Guinto, E.R. (2009) 'Elasto-anelastic regional structures of the crust and upper mantle beneath the Mediterranean basin derived from uncoupled causal inversion of Rayleigh wave attenuation coefficients and group velocities', in *EGU General Assembly Conference Abstracts*, Vol. 11, p.2420.

Martínez, M.D., Lana, X. and Guinto, E.R. (2010) 'Shear-wave attenuation tomography of the lithosphere-asthenosphere system beneath the Mediterranean region', *Tectonophysics*, Vol. 481, No. 1, pp.51–67.

Massa, M., Luzi, L., Pacor, F., Bindi, D. and Ameri, G. (2012) 'Comparison between empirical predictive equations calibrated at global and national scale and Italian strong-motion data', *Bollettino di Geofisica Teorica ed Applicata*, Vol. 53, No. 1, pp.37–53.

Meletti, C., Galadini, F., Valensise, G., Stucchi, M., Basili, R., Barba, S., Vannucci, G. and Boschi, E. (2008) 'A seismic source zone model for the seismic hazard assessment of the Italian territory', *Tectonophysics*, Vol. 450, No. 1, pp.85–108.

Morikawa, N. and Fujiwara, H. (2003) 'Source and path characteristics for off Tokachi-Nemuro earthquakes', in *Programme and Abstracts for the Seismological Society of Japan, 2003 Fall Meeting P*, Vol. 104.

NTC08 (2008) D*.M. 14 gennaio 2008 – Norme tecniche per le costruzioni*, Ministero delle Infrastrutture, in Italian, [online] http://www.cslp.it.

Panza, G.F., La Mura, C., Peresan, A., Romanelli, F. and Vaccari, F. (2012) 'Seismic hazard scenarios as preventive tools for a disaster resilient society', *Advances in Geophysics*, Vol. 53, pp.93–165.

Panza, G.F., Romanelli, F. and Vaccari, F. (2001) 'Seismic wave propagation in laterally heterogeneous anelastic media: theory and applications to seismic zonation', *Advances in Geophysics*, Vol. 43, pp.1–95.

Panza, G.F., Schwab, F.A. and Knopoff, L. (1973) 'Multimode surface waves for selected focal mechanisms – I. Dip-slip sources on a vertical fault plane', *Geophysical Journal of the Royal Astronomical Society*, Vol. 34, No. 3, pp.265–278.

Panza, G.F., Schwab, F.A. and Knopoff, L. (1975a) 'Multimode surface waves for selected focal mechanisms – II. Dip-slip sources', *Geophysical Journal of the Royal Astronomical Society*, Vol. 42, No. 3, pp.931–943.

Panza, G.F., Schwab, F.A. and Knopoff, L. (1975b) 'Multimode surface waves for selected focal mechanisms – III. Strike-slip sources', *Geophysical Journal of the Royal Astronomical Society*, Vol. 42, No. 3, pp.945–955.

Papageorgiou, A.S. and Aki, K. (1983) 'A specific barrier model for the quantitative description of inhomogeneous faulting and the prediction of strong ground motion. I. Description of the model', *Bulletin of the Seismological Society of America*, Vol. 73, No. 3, pp.693–722.

Parvez, I.A., Romanelli, F. and Panza, G.F. (2011) 'Long period ground motion at bedrock level in Delhi city from Himalayan earthquake scenarios', *Pure and Applied Geophysics*, Vol. 168, Nos. 3–4, pp.409–477.

Paskaleva I., Dimova, S., Panza, G.F. and Vaccari, F. (2007) 'An earthquake scenario for the microzonation of Sofia and the vulnerability of structures designed by use of the Eurocodes', *Soil. Dyn. Earthquake Eng*., Vol. 27, No. 11, pp.1028–1041.

Pavlov, V.M. (2009) 'Matrix impedance in the problem of the calculation of synthetic seismograms for a layered-homogeneous isotropic elastic medium', *Izvestiya Physics of the Solid Earth*, Vol. 45, No. 10, pp.850–860.

Pondrelli, S., Salimbeni, S., Ekström, G., Morelli, A., Gasperini, P. and Vannucci, G. (2006) 'The Italian CMT dataset from 1977 to the present', *Physics of the Earth and Planetary Interiors*, Vol. 159, No. 3, pp.286–303.

Pondrelli, S., Salimbeni, S., Morelli, A., Ekström, G., Olivieri, M. and Boschi, E. (2009) 'Seismic moment tensors of the April 2009, L'Aquila (Central Italy), earthquake sequence', *Geophysical Journal International*, Vol. 180, No. 1, pp.238–242.

Sabetta, F. and Pugliese, A. (1987) 'Attenuation of peak horizontal acceleration and velocity from Italian strong-motion records', *Bulletin of the Seismological Society of America*, Vol. 77, No. 5, pp.1491–1513.

Toro, G.R., Abrahamson, N.A. and Schneider, J.F. (1997) 'Model of strong ground motions from earthquakes in central and Eastern North America: best estimates and uncertainties', *Seismological Research Letters*, Vol. 68, No. 1, pp.41–57.

Uang, C. and Bertero, V. (1990) 'Evaluation of seismic energy in structures', *Earthquake Engineering and Structural Dynamics*, Vol. 19, No. 1, pp.77–90.

Vaccari, F. (2016) 'A web application prototype for the multiscale modelling of seismic input', in D'Amico, S. (Ed.): *Earthquakes and Their Impact on Society*, pp.563–584, Springer Natural Hazards, Springer International Publishing, Switzerland, DOI: 10.1007/978-3-319-21753-6_23.

Zuccolo, E., Vaccari, F., Peresan, A. and Panza, G.F. (2011) 'Neo-deterministic and probabilistic seismic hazard assessments: a comparison over the Italian territory', *Pure and Applied Geophysics*, Vol. 168, Nos. 1–2, pp.69–83.